Desalination and Water Treatment
www.deswater.com

doi: 10.5004/dwt.2022.28652

266 (2022) 276–283
August

Photodegradation of phenol under visible light using chabazite as a stabilizer in anatase TiO_2

Ildefonso Zamudio-Torres, Erik Ramírez-Morales, Germán Pérez-Hernández, María Guadalupe Hernández-Cruz, Lizeth Rojas-Blanco*

Universidad Juárez Autónoma de Tabasco, Avenida Universidad S/N, Col. Magisterial, Villahermosa, Tabasco, CP. 86040 México, Tel. +52-993-246-8500; Fax: +52-914-336-0940; emails: lizethrb@gmail.com/lizeth.rojas@ujat.mx (L. Rojas-Blanco), zit408@msn.com /ildefonso.zamudio@ujat.mx (I. Zamudio-Torres), eriking10@hotmail.com (E. Ramírez-Morales), gph08@hotmail.com/ german.perez@ujat.mx (G. Pérez-Hernández), guadalupe.hernandez@ujat.mx (M.G. Hernández-Cruz)

Received 2 March 2022; Accepted 10 June 2022

ABSTRACT

This work presents the synthesis of copper doped TiO_2 and the incorporation of zeolite by the sol–gel method. The obtained material had an admix of anatase and rutile phases, but incorporating zeolite leads to reaching just the anatase phase, that is, the zeolite stabilizes the anatase phase; however, it comes back to the admix phases when Cu is added in excess. The evaluation of the photocatalytic activity was using a phenol solution. The zeolite presence increased phenol adsorption, helping the photocatalysis process by adsorbing more phenol quickly, allowing the TiO_2 to act directly. The optimized percentage of zeolite was 1% (w/w), enhancing its photocatalytic activity under visible light compared to unmodified TiO_2. The Cu dopant incorporation in TiO_2 decreases its photoactivity in UV light but improves when it works under visible light. The optimal Cu incorporated on TiO_2 was 1% Cu (w/w), increasing its photocatalytic activity under visible light.

Keywords: Photocatalysis; TiO_2; Cu-doped TiO_2; Zeolite; Phenol

1. Introduction

Rapid industrialization and population growth have promoted the development of highly efficient, and green technology is now required to diminish worldwide challenges. As an advanced oxidation process, photocatalysis has fascinated with the photoreduction of heavy metals, air purification, and water treatment, due to its advantages of high efficacy, economic viability, and absence of secondary contamination [1–5].

TiO_2 is a widely researched material due to its high relevance in materials science applications and fundamental solid-state chemistry. This oxide has many uses, such as corrosion coating, anti-bacterial agent, air purification, surface cleaner, food additive, UV absorber in cosmetic products, or an opacifying agent in paints, plastics, paper, and dyes. It is also used to manufacture rechargeable batteries, supercapacitors, sensors, water remediation, and photocatalysis [6].

Multiple studies have emerged lately that focus on the photodegradation of pollutants [7–9]. Aguilar et al. [10] reported using TiO_2 without altering the material's structure; they modified its particle size and improved the adsorption capacity and photo efficiency.

Different authors have studied photodegradation mechanisms in the presence of pure and modified TiO_2 [11,12] to increase its absorption range in the electromagnetic spectra. Despite this, many studies about using TiO_2 and its composites [7,13–15]. Zeolite has been the most favorable material to be used as a support for TiO_2 since it has excellent photochemical stability, transparent to UV-VIS

* Corresponding author.

radiation (λ > 240 nm), and has better uniform pore distribution than alone TiO_2 [11,16,17].

Setthaya et al. [18] investigated the capacity of TiO_2 with zeolite for methylene blue removal, which can reduce the concentration of this pollutant close to 99%, increasing its photodegradation efficiency. These properties make zeolite an optimal material for increasing the amount of composite adsorption and facilitating the photocatalytic reaction.

TiO_2 can degrade contaminants by UV radiation and not with visible light. However, some authors have studied its photoactivity in visible light by introducing structural defects incorporating non-metallic compounds such as N, C, and S or specific metallic ions [19–21]. Cu is an essential dopant because it has high electronic conductivity, and it is very cheap with a high percentage on earth.

In some reports, Cu as a dopant reduces the energy bandgap of TiO_2 [22]. This reduction improves its photocatalytic efficiency in visible light, allowing the inactivation of certain microorganisms and the decomposition of organic pollutants such as methylene blue, methyl orange, or phenol [18,23–26]. Some authors reported the phenol photodegradation with supported TiO_2 to study whether it could take advantage of the visible spectrum [27,28].

This work presents the synthesis, structural characterization, and performance of Cu-doped TiO_2 as a photocatalyst, incorporating zeolite and its photocatalytic performance by degrading phenol under ultraviolet light and visible light. Furthermore, the influence of the chabazite in the TiO_2 structure as a stabilizer in the anatase phase is discussed.

2. Materials and methods

2.1. TiO_2 synthesis

The TiO_2 powders were prepared by sol–gel method, using the following amounts of reagents: 13 mL of titanium butoxide ($Ti[OBu]_4$, Sigma-Aldrich, 97%), 1 mL of distilled water (H_2O, 18 MΩ-cm), 45 mL of ethanol (EtOH, Sigma-Aldrich 99.5%). The synthesis starts by mixing H_2O and EtOH, then adding $Ti(OBu)_4$ to obtain the sol. This resultant solution was stirred vigorously at 200 rpm, at normal environment conditions for 1 h; after that, the reaction gives hydrolysis and polycondensation, generating a viscous wet gel. Then, this gel was dried at 100°C in an oven for 12 h, and finally, the resultant material was annealed at 550°C for 2 h to remove the remaining water and all organic content.

2.2. Cu-doped TiO_2 synthesis and incorporation of zeolite chabazite

Previous, the zeolite was milled using agate mortar, then it was added into a flask and washed with deionized water (1:4 rate in water) with vigorous constant stirring (350 rpm) for 24 h; then, the zeolite was dried and annealing inside an oven at 250°C during 4 h. The Al and Si elements from chabazite zeolite were removed by washing with HCl (ACS Reagent, 37%) and NH_4Cl (ACS Reagent, 99.5%) solutions at 0.5 M, respectively; for this purpose, it was stirred for 20 min twice. This Al and Si remotion process creates vacancies in the chabazite zeolite structure, increasing the adsorption capacity. After that, the zeolite was dried in an oven at 120°C for 4 h.

The synthesis of Cu-doped TiO_2 on zeolite involved the preparation of two solutions which are: Solution 1 was made: dissolving $Cu(NO_3)_2$ (Sigma-Aldrich, 99.9%) at 0.5% w/w or 1% w/w in a mixture of deionized water and EtOH with 2.7 and 10 mL, respectively. Solution 2: chabazite zeolite, 1% w/w or 5% w/w, was dispersed in a mixture of $Ti[OBu]_4$ and HCl with 13 and 1 mL, respectively. The weight percentages concern the precursor of Ti.

The hydrolysis and polycondensation reactions obtained the Cu-doped TiO_2 on zeolite. For this purpose, solution one was added dropwise to solution two slowly; this step's duration was 12–15 min. After that, the resultant solution was maintained at stirring for 1 h to obtain a homogeneous gel. Afterward, the remaining water and alcohol were dried by heating at 100°C for 12 h, up to the obtained powder. Then, this powder was milled and finally annealed at 550°C for 2 h to remove the remaining water and organic compounds content. According to the Cu precursor content (0.5 wt.% or 1 wt.%) and zeolite content (1 wt.% and 5 wt.%) quantities, the as-synthesized materials were named as shown in Table 1.

2.3. Characterization techniques

The photocatalysts' structural properties were determined by a Rigaku X-ray diffractometer, SmartLab model, using monochromatized Cu Kα radiation (λ = 1.54056 Å). X-ray diffraction (XRD) patterns were collected using a scan speed of 2 s/step, with 0.05°/steps, from 20° to 70° (2θ) using razing incident beam at fix angle of 0.6°. The acceleration voltage and current were 40 kV and 44 mA, respectively.

Raman spectra of catalysts were acquired using a micro–Raman Dilor LabRam, model II, equipped with an optical microscope at 50X objective magnification, using a laser beam wavelength of 632.8 nm. The sample was focused on a spot size of ~5 μm in diameter. The acquisition was from 100 to 700 cm^{-1}, but before measurement, the system was calibrated using polycrystalline Si, centering the Raman peak at 520 cm^{-1}.

FT-IR spectra were measured through a Shimadzu spectrophotometer (model IRAffinity-1). The data were collected from 400 to 4,000 cm^{-1}, at operating conditions of 1000 scans with 4 cm^{-1} resolution in transmittance mode, to identify functional groups present for all samples.

The materials' optical absorption and the remaining phenol concentration during its degradation were recorded

Table 1
Labels of the samples obtained and its contents weight percent of Cu and zeolite used in the synthesis

Name	Cu wt.%	Zeolite wt.%
TiO_2	0	0
TZ1	0	1
TZ5	0	5
TC0.5Z1	0.5	1
TC0.5Z5	0.5	5
TC1Z1	1	1
TC1Z5	1	5

in a diffuse reflectance mode with a wavelength range from 200 nm to 700 nm, using a Shimadzu UV-VIS spectrophotometer (model UV-2600). The bandgap value of the samples was determined from their diffuse reflectance by plotting the transformed Kubelka-Munk equation vs. photon energy ($E = h\nu$); this equation is as follows:

$$F(R) = \frac{(1-R)^2}{2R}$$

where R is the diffuse reflectance, and F(R) is the absorbance [29].

2.4. Photocatalysis tests

The photocatalytic activity of the materials was evaluated by the degradation of phenol in an aqueous solution at 40 ppm concentration (C_6H_5OH, 98.8%, Alfa Aesar), at constant stirring. The tests were carried out by adding 0.03 g of catalyst to 60 mL of the phenol solution.

The photocatalytic reactor has a 20 W Tecno Lite lamp with UV–Vis emission (250–380 nm) and a 50 W Smartlight MR-16EXN lamp to simulate the visible light (480 nm–650 nm). The experiment was closed off to avoid the contribution of external light. The absorbance spectra of the solution were monitored every 30 min for 5 h, using a Shimadzu UV-VIS spectrophotometer (model UV-2600). The intensity variation of the main band localized at 270 nm was co-related with the degradation of phenol.

3. Results discussion

3.1. Structural characterization

3.1.1. X-ray diffraction

The XRD patterns are shown in Fig. 1a and b, corresponding to all synthesized catalysts. This technique demonstrates the existence of the anatase phase with principal intensities (101), (004), (200), (105), (211), and (204). It was indexed using JCPDS Card no. 21-1272 for all materials.

Fig. 1a shows patterns for the samples TiO_2, TZ1, and TZ5. The pattern for TiO_2 shows the principal intensities for the anatase phase. However, it shows intensities that correspond to the rutile phase indexed with the JCPDS Card no. 21-1276, and there are present (110), (101), (211), and (301) intensities. Therefore, the TiO_2 sample contains a admix of both phases, anatase, and rutile.

It can be noticed in the samples TZ1 and TZ5, which contain zeolite, the rutile phase is absent, and its lack is due to a dilution effect of the zeolite matrix in the catalyst [9]. Furthermore, the amount of water-alcohol solution used for hydrolysis during sol–gel synthesis (when the zeolite is used), ethanol decreases, and the acidity of sol increases; consequently, the chelation effect is higher [30]. An increment in chelation results in a strong gel network, and therefore, the growth of the anatase phase is mainly promoted [31].

Fig. 1b shows the X-ray patterns for the samples TC0.5Z1, TC1Z1, TC0.5Z5, and TC1Z5. It is possible to recognize the anatase phase for all samples; furthermore, there are no intensities from other phases, such as intensities corresponding to Cu oxide and others; this could indicate the presence of Cu is an amorphous phase or highly dispersed on the TiO_2 surface, consistently with previous reports [32,33]. However, in the sample TC1Z5, intensities (110) and (101) suggest the rutile phase (indicated by arrows). Besides, this sample contains the most Cu weight percentage used, leading to the conversion of anatase to rutile by Cu doping [15]. The above experimental results make it possible to infer Cu dopes the TiO_2, and incorporating zeolite helps stabilize the anatase phase, but only when the wt.% of Cu and zeolite precursors is less than one and greater than 1, respectively.

3.1.2. Raman spectroscopy

Fig. 2 shows the Raman spectra for all study materials. Fig. 2a shows the intensities at 140 and 636 cm^{-1}, corresponding to E_g mode oscillation of TiO_2 with anatase phase; these signals arise due to the symmetrical stretching vibration of O–Ti–O. The intensity at 197 cm^{-1} is due to the E_g mode (see the inset), present in the anatase phase. The peak at 394 cm^{-1} corresponds to the B1g mode of the anatase, which arises by asymmetrical bending vibrations of O–Ti–O [7]. The intensity at 514 cm^{-1} corresponds to the A1g mode of anatase, which occurs by symmetrical O–Ti–O bending vibrations.

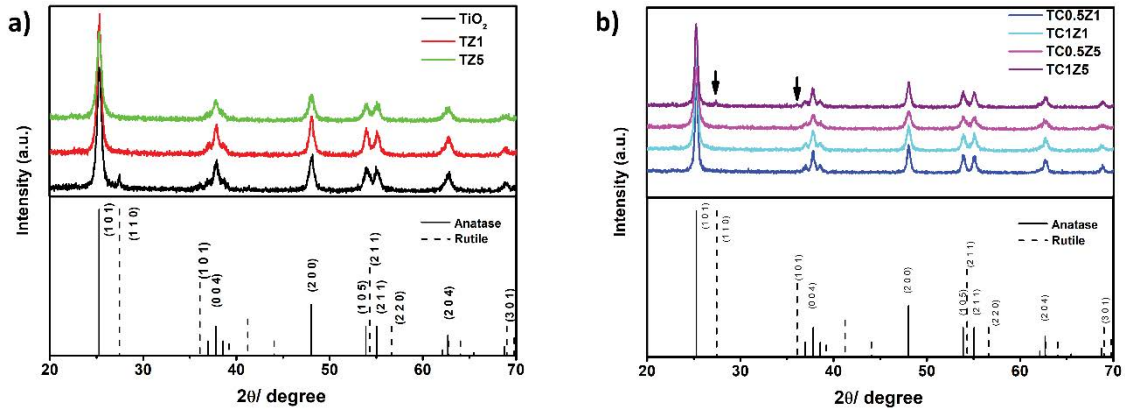

Fig. 1. X-ray diffractogram for the samples (a) TiO_2, TZ1, and TZ5 and (b) TiO_2 compared with TC0.5Z1, TC1Z1, TC0.5Z5, and TC1Z5. The samples show planes of the anatase and rutile phase or just anatase.

The slight red shift of the spectra for samples TZ1 and TZ5 is due to zeolite distribution through TiO_2 [34].

Fig. 2b shows intensities corresponding to the TiO_2 in samples containing Cu and zeolite. At 264 cm^{-1}, the Ag mode of Cu–O due to Cu doping in the TiO_2 matrix is visible, causing displacement for spectra TC0.5Z1, TC1Z1, TC0.5Z5, and TC1Z5 [35]. The doping occurs because Cu is a free ion when reacting in the gel assembly. It binds to the structure's oxygen, forming Cu–O–Ti or Cu–O–Cu; this presence could potentiate photocatalytic activity. Doping occurs mainly by replacing Ti^{4+} in the Ti–O–Ti bonds with Cu^{2+}, visualizing disorders in the Raman spectrum, as previously reported [6,15]. The difference in charges between Ti^{4+} and Cu^{2+} ions raises oxygen vacancies in the lattice of the TiO_2 structure to keep the charge of the neutral compound [36]. Therefore, complementing the XRD patterns study, the samples TC0.5Z1, TC1Z1, TC0.5Z5, and TC1Z5 are doped by Cu.

3.1.3. FT-IR spectroscopy

FTIR spectra (Fig. 3a) show the characteristic bands from 500 to 4,000 cm^{-1} to analyze the functional groups present in the materials obtained. Throughout the transmittance of the material measured and the different intensities observed, it was possible to establish each molecule's vibrational state in the sample. The composition of the samples can be known as in-depth as its degree of purity.

The intensities around 3,435 cm^{-1} correspond to the presence of OH ions due to stretching vibrations. The intensities at 2,372 and 2,312 cm^{-1} correspond to water molecules due to exposure to the environment. The peak localized at 1,630 cm^{-1} corresponds to the OH bonds' existing deformation, which originates from the water molecules abovementioned [34,37,38]. These last three intensities are not so prominent since the heat treatment removed all water and excess ethanol from the synthesis processes. Hence, it is possible to conclude that their presence is due exclusively to the presence of water in the atmosphere due to the material's porosity; this characteristic allows this phenomenon to occur. Furthermore, it is possible to observe intensities between 969 and 1,221 cm^{-1}, corresponding to the tetrahedral formations of Si from the asymmetrical stretching vibrations that exist in these structures, which correspond to the presence of zeolite. Intensities at 476 and 651 cm^{-1} are

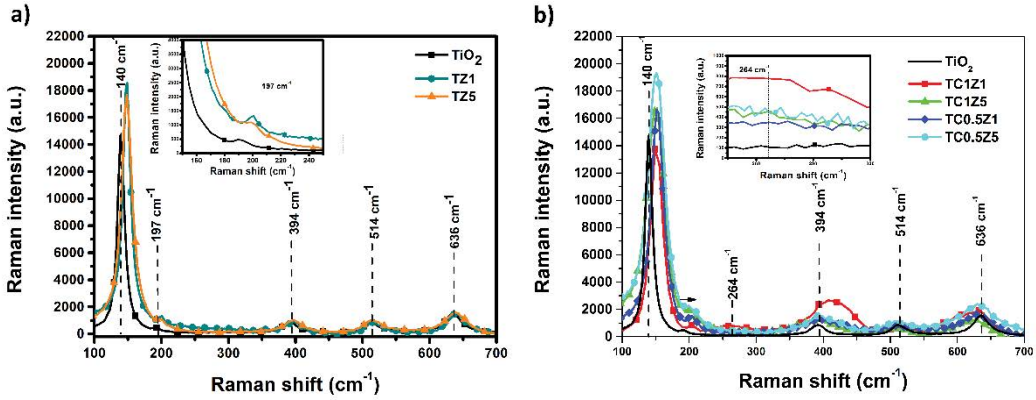

Fig. 2. Raman spectra for the samples (a) TiO_2, TZ1, and TZ5 and (b) TiO_2 compared with TC0.5Z1, TC1Z1, TC0.5Z5, and TC1Z5. Spectra show the intensities for the anatase and rutile phases. The displacement (arrow in b) indicates the anatase phase. Inset zoom figures are shown in the detail of intensity variations.

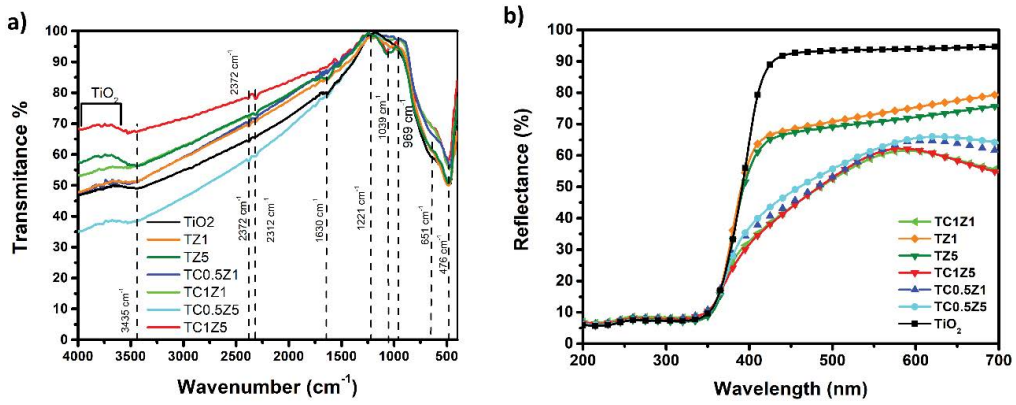

Fig. 3. (a) Transmittance spectra for the samples TiO_2, TZ1, and TZ5, TC0.5Z1, TC1Z1, TC0.5Z5, and TC1Z5 show the wavenumber identified for the functional groups present in each sample and (b) shows the reflectance (%) spectra for the catalysts in the range from 200 to 700 nm.

by vibrations generated by Ti–O and Cu–O, respectively, and the combination of them.

The presence of copper improves transmittance slightly due to the rate of Cu weight used. Therefore, Cu-doped TiO_2 better the light transmittance [15,18,33,39].

3.1.4. Optical characterization (reflectance)

Fig. 3b shows the reflectance spectra of the obtained samples. It can be noticed that the TZ1 and TZ5 samples show a decrease in reflectance of visible light (400–700 nm) compared to TiO_2, generating an increase in absorption light. The samples TC0.5Z1, TC0.5Z5, TC1Z1, TC1Z5 decrease up to 40% more in reflectance for visible light, potentializing its photocatalytic characteristics due to the rate weight Cu used in the synthesis process. This behavior is positive to achieve the purpose of this work.

The values of the energy bands were obtained by the extrapolation of the straight-line plot of $[F(R)E]^{1/2}$ vs. photon energy [40], considering that TiO_2 has a direct band transition. These bandgap values are present in Table 2. As these can be seen, there are no significant changes in values (3.36 ± 0.02 eV).

3.1.5. Photocatalysis behavior

3.1.5.1. Under UV radiation

Fig. 4 shows the photocatalyst behavior of all synthesized samples. These graphs show the plot C/C_0 vs. time, where C is concentration in a time interval, and C_0 is the initial concentration of a phenol solution (40 ppm) reacting with the photocatalyst (30 mg). Also, it is possible to observe that the plots start at time –1 h due to the reaction being isolated from any light source for 1 h. This step is to estimate the adsorption capacity of the corresponding catalyst. The plots show that the samples TZ5, TC0.5Z5, and TC1Z5 adsorb the phenol better due to the adsorption capacity of the zeolite. Sample TZ5 contains the highest amount of zeolite (Table 1), showing the adsorption capacity of the zeolite.

Fig. 4a shows the phenol solution rate degradation for 5 h under UV light irradiation (a) and visible light (b). In this plot, it is possible to observe that sample TZ1 shows better results with a final removal of 31.56%, followed by the sample labeled as TiO_2, with total removal of 26.27% at the same time (Table 3). It indicates that adding 1% of zeolite to TiO_2 allows good initial adsorption, helping considerably in the photocatalytic process.

The sample TZ5 reached 16.65% in the photodegradation of phenol, and this value is less than sample TZ1. This behavior is related to the reduction in the active surface of TiO_2 by increasing the zeolite concentration adhered to the matrix of the material (5% w/w zeolite in TZ5). According to Durgakumari et al. [27], the interaction between TiO_2

Table 2
Bandgap values determined for obtained samples

Sample	E_g (eV)
TiO_2	3.38
TZ1	3.38
TZ5	3.37
TC0.5Z1	3.36
TC0.5Z5	3.37
TC1Z1	3.35
TC1Z5	3.35

Table 3
Degradation percentage after 5 h under UV and visible light irradiation for all samples

Sample	Phenol remotion (%) during 5 h under light source	
	UV	Vis
TiO_2	26.27	8.08
TZ1	31.56	8.55
TZ5	16.65	5.04
TC0.5Z1	10.83	5.35
TC0.5Z5	14.45	9.89
TC1Z1	8.22	11.68
TC1Z5	13.12	10.95

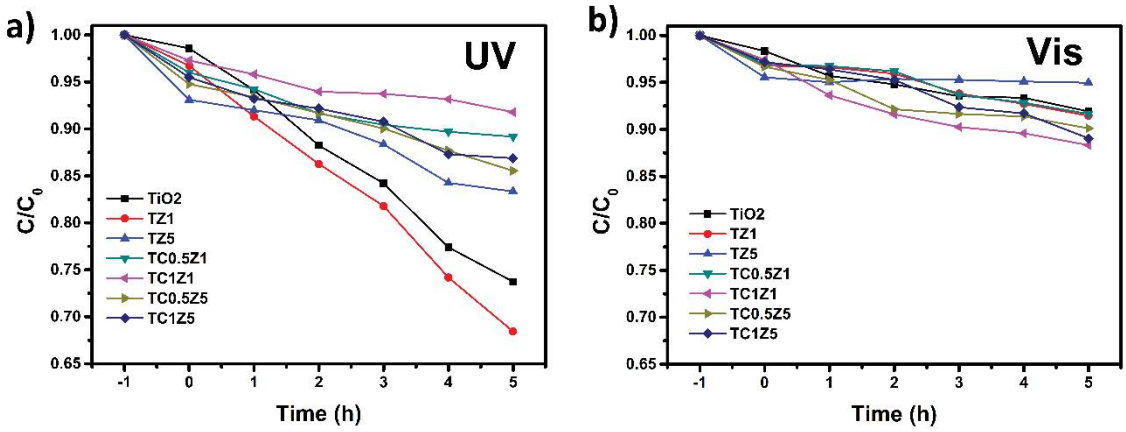

Fig. 4. Plots of the photocatalytic activity for 5 h for (a) under UV light and (b) under visible light.

and zeolite could decrease the photocatalytic activity, but at sufficient concentration, it could improve its photoactivity.

The zeolite itself plays the role of an adsorber of molecules, accelerating the TiO_2 activity, but by increasing the zeolite concentration, it immobilizes the TiO_2, causing a decrease in its photoefficiency [27]. Therefore, the zeolite helps increase the adsorption capacity of the material, but to the detriment of photocatalytic efficiency [23].

However, when TiO_2 doped with Cu and zeolite was incorporated, the samples showed poor photo efficiency; this behavior is related to the presence of Cu^{2+} species, as previously confirmed with Raman characterization. According to Colón et al. [41], this species consumes/receives a photogenerated electron from the TiO_2 conduction band, leading it to Cu^{+}; this avoids the formation of $OH^{\bullet}$ radicals. The rapid reduction from Cu^{2+} to Cu^{+} when the TiO_2 is photoexcited makes Cu^{+} nonstable, forming once again Cu^{2+}, generating a recombination process.

3.1.5.2. Under visible light radiation

Fig. 4b shows the photocatalytic activity under visible light. The sample TZ5 has the lowest degradation efficiency (5.04%) due to the zeolite immobilizing the TiO_2 [27], inclusive its performance is lesser than TiO_2 (8.08%), followed by TZ1 (8.55%). In this case, the sample TC1Z1 showed the best performance with a total remotion of 11.68%, followed by TC1Z5 and TC0.5Z5 with the removal of 10.95% and 9.89%, respectively (Table 3 and Fig. 4b).

The Cu incorporated in the structures modified the optical absorption of the TiO_2 on zeolite considerably, allowing them to take better advantage of the visible light irradiation due to its lower reflectance than the TiO_2, as discussed in Fig. 3. The TZ1 and TZ5 samples were able to adsorb phenol at the beginning of the photocatalysis tests due to the zeolite adsorption capacity. The composites with the lowest amount of zeolite (1%) were able to absorb a considerable amount of phenol without changing the photocatalytic capacity of the materials compared to TiO_2. On the other hand, the samples with 5% of zeolite adsorbed a higher amount of phenol but considerably affected the photocatalytic activity of the samples. As could be seen, the zeolite had the same effect as in the tests under UV light, showing an increase in phenol adsorption and reducing its photocatalytic activity by increasing the zeolite quantity.

The best results were the TC1Z1 sample due to the Cu allowing phenol degradation in the visible light and zeolite allowing more adsorption in less time without altering the photocatalytic characteristics of Cu-doped TiO_2.

From the above, it can be noticed that the incorporation of Cu is not recommendable if the degradation will be under UV light; it is due to the samples with Cu content higher than 1% having poor results. On the other hand, the ideal concentration of chabazite zeolite to improve phenol degradation is 1% due to its ability to adsorbs the right amount of phenol without compromising the photocatalytic properties of the material.

To understand the activity photocatalytic of TiO_2 – chabazite, is speculated the following mechanism: first, chabazite acts as an effective adsorbent to condense pollutants molecules, which is one of the significant reaction steps in degradation [42]. Under the illumination of UV light, TiO_2 on the surface of chabazite is activated, generating electron–hole pairs (1). Then, when the electron–hole pairs react with H_2O (2) and (3) or O_2 (4), reactive species such as $OH^{\bullet}$ and O_2^- are formed, respectively. And these active species work for the photodegradation of the pollutant, oxidation products when holes act (6), and reduction products when electrons work (7) [43,44]. Finally degraded to CO_2, H_2O, and other micromolecules [45].

$$TiO_2 + h\upsilon(UV) \rightarrow TiO_2(e^-) + TiO_2(h^+) \quad (1)$$

$$TiO_2(h^+) + H_2O \rightarrow TiO_2 + H^+ + OH^{\bullet} \quad (2)$$

$$TiO_2(h^+) + OH^- \rightarrow TiO_2 + OH^{\bullet} \quad (3)$$

$$TiO_2(e^-) + O_2 \rightarrow TiO_2 + O_2^- \quad (4)$$

$$O_2^- + H^+ \rightarrow OH^{\bullet} \quad (5)$$

$$2h^+ + H_2O \rightarrow 1/2O_2 + 2H^+ \quad (6)$$

$$2e^- + 2H^+ \rightarrow H_2 \quad (7)$$

4. Conclusions

By the sol–gel synthesis method was possible to obtain Cu-doped TiO_2 and incorporate zeolite as a stabilizer of the anatase phase. It confirmed the role of zeolite in the phenol adsorption process, improving the photocatalysis activity of TiO_2 directly. Increasing the zeolite concentration quantity immobilizes TiO_2, which decreases its photoefficiency. The optimum quantity of zeolite incorporated into TiO_2 was 1% (w/w); this value does not compromise its photocatalytic activity but improves its adsorption capacity to find a better photocatalytic activity of the compound material. The Cu-doped TiO_2 decreases its photoactivity under UV irradiation. However, the presence of Cu dopant enhances its photocatalytic activity of TiO_2 under visible light, with 1% (w/w) as the optimal quantity. The material with the optimum quantity of dopant and zeolite is ready for any contaminant degradation by the photocatalytic process.

Acknowledgments

The authors gratefully acknowledge the financial support from the Mexican Council for Science and Technology (CONACyT, Grant CB-SEP-CONACYT No. 286165) and Universidad Juárez Autónoma de Tabasco (UJAT, internal fund, Grant No.765), and the PRODEP fund UJAT–PTC–296.

References

[1] B. Liu, X. Liu, J. Liu, C. Feng, Z. Li, C. Li, Y. Gong, L. Pan, S. Xu, C.Q. Sun, Efficient charge separation between UiO-66 and $ZnIn_2S_4$ flowerlike 3D microspheres for photoelectronchemical properties, Appl. Catal., B, 226 (2018) 234–241.

[2] T. Ni, Z. Yang, H. Zhang, L. Zhou, W. Guo, L. Pan, Z. Yang, K. Chang, C. Ge, D. Liu, Peroxymonosulfate activation by Co_3O_4/SnO_2 for efficient degradation of ofloxacin under visible light, J. Colloid Interface Sci., 615 (2022) 650–662.

[3] D. Liu, C. Li, J. Ge, C. Zhao, Q. Zhao, F. Zhang, T. Ni, W. Wu, 3D interconnected g-C_3N_4 hybridized with 2D Ti_3C_2 MXene nanosheets for enhancing visible light photocatalytic hydrogen evolution and dye contaminant elimination, Appl. Surf. Sci., 579 (2022) 152180, doi: 10.1016/j.apsusc.2021.152180.

[4] D. Liu, H. Li, R. Gao, Q. Zhao, Z. Yang, X. Gao, Z. Wang, F. Zhang, W. Wu, Enhanced visible light photoelectrocatalytic degradation of tetracycline hydrochloride by I and P co-doped TiO_2 photoelectrode, J. Hazard. Mater., 406 (2021) 124309, doi: 10.1016/j.jhazmat.2020.124309.

[5] D. Liu, C. Li, C. Zhao, Q. Zhao, T. Niu, L. Pan, P. Xu, F. Zhang, W. Wu, T. Ni, Facile synthesis of three-dimensional hollow porous carbon doped polymeric carbon nitride with highly efficient photocatalytic performance, Chem. Eng. J., 438 (2022) 135623, doi: 10.1016/j.cej.2022.135623.

[6] Y. Liu, C. Xu, Y. Xie, L. Yang, Y. Ling, L. Chen, Au–Cu nanoalloy/TiO_2/MoS_2 ternary hybrid with enhanced photocatalytic hydrogen production, J. Alloys Compd., 820 (2020) 153440, doi: 10.1016/j.jallcom.2019.153440.

[7] S. Jadhav, R. Navarro-Mendoza, P. Lozano-Sotomayor, I.R. Galindo-Esquivel, O. Serrano, J.M. Peralta-Hernández, Enhanced photocatalytic activity of TiO_2 modified with GaI toward environmental application, Inorg. Chem., 59 (2020) 1315–1322.

[8] C.Y. Kuo, C.H. Wu, H.Y. Lin, Synergistic effects of TiO_2 and Cu_2O in UV/TiO_2/zeolite-based systems on photodegradation of bisphenol A, Environ. Technol. (United Kingdom), 35 (2014) 1851–1857.

[9] S. Gomez, C.L. Marchena, L. Pizzio, L. Pierella, Preparation and characterization of TiO_2/HZSM-11 zeolite for photodegradation of dichlorvos in aqueous solution, J. Hazard. Mater., 258–259 (2013) 19–26.

[10] T. Aguilar, J. Navas, R. Alcántara, C. Fernández-Lorenzo, J.J. Gallardo, G. Blanco, J. Martín-Calleja, A route for the synthesis of Cu-doped TiO_2 nanoparticles with a very low bandgap, Chem. Phys. Lett., 571 (2013) 49–53.

[11] Y. Zhao, J. Li, L. Wang, Y. Hao, L. Yang, P. He, J. Xue, Preparation and characterization of sulfated TiO_2/zeolite composite catalysts with enhanced photocatalytic activity, Nano, 13 (2018) 1850117, doi: 10.1142/S1793292018501175.

[12] W. Donphai, T. Kamegawa, M. Chareonpanich, K. Nueangnoraj, H. Nishihara, T. Kyotani, H. Yamashita, Photocatalytic performance of TiO_2–zeolite templated carbon composites in organic contaminant degradation, Phys. Chem. Chem. Phys., 16 (2014) 25004–25007.

[13] X. Liu, Y. Liu, S. Lu, W. Guo, B. Xi, Performance and mechanism into TiO_2/zeolite composites for sulfadiazine adsorption and photodegradation, Chem. Eng. J., 350 (2018) 131–147.

[14] F. Liu, X. Ma, H. Li, Y. Wang, P. Cui, M. Guo, H. Yaxin, W. Lu, S. Zhou, M. Yu, Dilute sulfonic acid post functionalized metal organic framework as a heterogeneous acid catalyst for esterification to produce biodiesel, Fuel, 266 (2020) 117149, doi: 10.1016/j.fuel.2020.117149.

[15] Z. Xiong, Z. Xu, Y. Li, L. Dong, J. Wang, J. Zhao, X. Chen, Y. Zhao, H. Zhao, J. Zhang, Incorporating highly dispersed and stable Cu^+ into TiO_2 lattice for enhanced photocatalytic CO_2 reduction with water, Appl. Surf. Sci., 507 (2020) 145095, doi: 10.1016/j.apsusc.2019.145095.

[16] K. Guesh, Á. Mayoral, Y. Chebude, M.J. López-Muñoz, C. Márquez-Álvarez, I. Diaz, Effect of thermal treatment on the photocatalytic behavior of TiO_2 supported on zeolites, New J. Chem., 42 (2018) 12001–12007.

[17] M. Castañeda-juárez, V. Martínez-miranda, P.T. Almazán-sánchez, Synthesis of TiO_2 catalysts doped with Cu, Fe, and Fe/Cu supported on clinoptilolite zeolite by an electrochemical-thermal method for the degradation of diclofenac by heterogeneous photocatalysis, J. Photochem. Photobiol., A, 380 (2019) 111834, doi: 10.1016/j.jphotochem.2019.04.045.

[18] N. Setthaya, P. Chindaprasirt, S. Yin, K. Pimraksa, TiO_2-zeolite photocatalysts made of metakaolin and rice husk ash for remoal of methylene blue dye, Powder Technol., 313 (2017) 417–426.

[19] J. Hu, J. Xie, W. Jia, S. Zhang, S. Wang, K. Wang, Y. Cao, Interesting molecule adsorption strategy induced energy band tuning: boosts 43 times photocatalytic water splitting ability for commercial TiO_2, Appl. Catal., B, 268 (2020) 118753, doi: 10.1016/j.apcatb.2020.118753.

[20] C. Wang, Y. Li, Preparation and characterisation of S doped TiO_2/natural zeolite with photocatalytic and adsorption activities, Mater. Technol., 29 (2014) 204–209.

[21] C. Wang, H. Shi, Y. Li, Synthesis and characterization of natural zeolite supported Cr-doped TiO_2 photocatalysts, Appl. Surf. Sci., 258 (2012) 4328–4333.

[22] H. Lee, H.S. Jang, N.Y. Kim, J.B. Joo, Cu-doped TiO_2 hollow nanostructures for the enhanced photocatalysis under visible light conditions, J. Ind. Eng. Chem., 99 (2021) 352–363.

[23] N. Chaouati, A. Soualah, M. Chater, Adsorption of phenol from aqueous solution onto zeolites Y modified by silylation, C.R. Chim., 16 (2013) 222–228.

[24] W. Zhang, X. Xiao, L. Zheng, C. Wan, Fabrication of TiO_2/MoS_2@zeolite photocatalyst and its photocatalytic activity for degradation of methyl orange under visible light, Appl. Surf. Sci., 358 (2015) 468–478.

[25] C.S. Uyguner Demirel, N.C. Birben, M. Bekbolet, A comprehensive review on the use of second generation TiO_2 photocatalysts: microorganism inactivation, Chemosphere, 211 (2018) 420–448.

[26] A. Taheri Najafabadi, F. Taghipour, Cobalt precursor role in the photocatalytic activity of the zeolite-supported TiO_2-based photocatalysts under visible light: a promising tool toward zeolite-based core-shell photocatalysis, J. Photochem. Photobiol., A, 248 (2012) 1–7.

[27] V. Durgakumari, M. Subrahmanyam, K. Subba Rao, A. Ratnamala, M. Noorjahan, K. Tanaka, An easy and efficient use of TiO_2 supported HZSM-5 and TiO_2+HZSM-5 zeolite combinate in the photodegradation of aqueous phenol and *p*-chlorophenol, Appl. Catal., A, 234 (2002) 155–165.

[28] P. Górska, A. Zaleska, J. Hupka, Photodegradation of phenol by UV/TiO_2 and Vis/N,C-TiO_2 processes: COMPARATIVE mechanistic and kinetic studies, Sep. Purif. Technol., 68 (2009) 90–96.

[29] H. Jamil, I.M. Dildar, U. Ilyas, J.Z. Hashmi, S. Shaukat, M.N. Sarwar, M. Khaleeq-ur-Rahman, Microstructural and optical study of polycrystalline manganese oxide films using Kubelka–Munk function, Thin Solid Films, 732 (2021) 138796, doi: 10.1016/j.tsf.2021.138796.

[30] N.T. Nolan, M.K. Seery, S.C. Pillai, Spectroscopic investigation of the anatase -to-rutile transformation of sol-gel-synthesized TiO_2 photocatalysts, J. Phys. Chem. C, 113 (2009) 16151–16157.

[31] N.D. Johari, Z.M. Rosli, J.M. Juoi, S.A. Yazid, Comparison on the TiO_2 crystalline phases deposited via dip and spin coating using green sol–gel route, J. Mater. Res. Technol., 8 (2019) 2350–2358.

[32] H. Abdelouahab Reddam, R. Elmail, S. Cerro Lloria, G. Monrós Tomás, Z. Abdelouahab Reddam, F. Coloma-Pascual, Synthesis of Fe, Mn and Cu modified TiO_2 photocatalysts for photodegradation of Orange II, Bol. Soc. Esp. Ceram. Vidrio, 59 (2020) 138–148.

[33] L. Zhang, B. Han, P. Cheng, Y.H. Hu, *In-situ* FTIR-DRS investigation on shallow trap state of Cu-doped TiO_2 photocatalyst, Catal. Today, 341 (2020) 21–25.

[34] K.M. Alvarez, J. Alvarado, B.S. Soto, M.A. Hernandez, Synthesis of TiO_2 nanoparticles and TiO_2-zeolite composites and study of optical properties and structural characterization, Optik (Stuttg), 169 (2018) 137–146.

[35] Z. Hai, C. Zhu, J. Huang, H. Liu, J. Chen, Controllable synthesis of CuO nanowires and Cu_2O crystals with shape evolution via γ-irradiation, Inorg. Chem., 49 (2010) 7217–7219.
[36] S. Zhu, X. Chen, Z. Li, X. Ye, Y. Liu, Y. Chen, L. Yang, M. Chen, D. Zhang, G. Li, H. Li, Cooperation between inside and outside of TiO_2: lattice Cu^+ accelerates carrier migration to the surface of metal copper for photocatalytic CO_2 reduction, Appl. Catal., B, 264 (2020) 118515, doi: 10.1016/j.apcatb.2019.118515.
[37] M.R.F. dos Santos, A.M.G. Pedrosa, M.J.B. de Souza, Oxidative desulfurization of thiophene on TiO_2/ZSM-12 zeolite, Mater. Res., 19 (2016) 24–30.
[38] X. Liu, Y. Liu, S. Lu, W. Guo, B. Xi, Performance and mechanism into TiO_2/zeolite composites for sulfadiazine adsorption and photodegradation, Chem. Eng. J., 350 (2018) 131–147.
[39] X.J. Liu, L.K. Pan, Z. Sun, Y.M. Chen, X.X. Yang, L.W. Yang, Z.F. Zhou, C.Q. Sun, Strain engineering of the elasticity and the Raman shift of nanostructured TiO_2, J. Appl. Phys., 110 (2011) 044322, doi: 10.1063/1.3626044.
[40] G.N. Shao, S.M. Imran, S.J. Jeon, M. Engole, N. Abbas, M. Salman Haider, S.J. Kang, H.T. Kim, Sol–gel synthesis of photoactive zirconia–titania from metal salts and investigation of their photocatalytic properties in the photodegradation of methylene blue, Powder Technol., 258 (2014) 99–109.
[41] G. Colón, M. Maicu, M.C. Hidalgo, J.A. Navío, Cu-doped TiO_2 systems with improved photocatalytic activity, Appl. Catal., B, 67 (2006) 41–51.
[42] G. Zhang, A. Song, Y. Duan, S. Zheng, Enhanced photocatalytic activity of TiO_2/zeolite composite for abatement of pollutants, Microporous Mesoporous Mater., 255 (2018) 61–68.
[43] V.M. Daskalaki, M. Antoniadou, G. Li Puma, D.I. Kondarides, P. Lianos, Solar light-responsive Pt/CdS/TiO_2 photocatalysts for hydrogen production and simultaneous degradation of inorganic or organic sacrificial agents in wastewater, Environ. Sci. Technol., 44 (2010) 7200–7205.
[44] Y. Wang, J. Chen, X. Lei, Y. Ren, Preparation of microporous zeolites TiO_2/SSZ-13 composite photocatalyst and its photocatalytic reactivity, Microporous Mesoporous Mater., 250 (2017) 9–17.
[45] N.S. Kovalevskiy, M.N. Lyulyukin, D.S. Selishchev, D.V. Kozlov, Analysis of air photocatalytic purification using a total hazard index: effect of the composite TiO_2/zeolite photocatalyst, J. Hazard. Mater., 358 (2018) 302–309.